Depth profiling and imaging capabilities of an ultrashort pulse laser ablation time of flight mass spectrometer

Yang Cui (崔扬),[1] Jerry F. Moore,[2] Slobodan Milasinovic,[1] Yaoming Liu (刘耀明),[1] Robert J. Gordon,[1] and Luke Hanley[1,a)]
[1]*Department of Chemistry, University of Illinois at Chicago, Chicago, Illinois 60607, USA*
[2]*MassThink LLC, 500 E. Ogden Ave., Suite 200, Naperville, Illinois 60563, USA*

(Received 14 June 2012; accepted 22 August 2012; published online 11 September 2012)

An ultrafast laser ablation time-of-flight mass spectrometer (AToF-MS) and associated data acquisition software that permits imaging at micron-scale resolution and sub-micron-scale depth profiling are described. The ion funnel-based source of this instrument can be operated at pressures ranging from 10^{-8} to ~0.3 mbar. Mass spectra may be collected and stored at a rate of 1 kHz by the data acquisition system, allowing the instrument to be coupled with standard commercial Ti:sapphire lasers. The capabilities of the AToF-MS instrument are demonstrated on metal foils and semiconductor wafers using a Ti:sapphire laser emitting 800 nm, ~75 fs pulses at 1 kHz. Results show that elemental quantification and depth profiling are feasible with this instrument. © *2012 American Institute of Physics*. [http://dx.doi.org/10.1063/1.4750974]

I. INTRODUCTION

Laser ablation with ultrashort pulses has the remarkable ability to remove material from the surface layer of a solid while doing minimal damage to the remaining sample.[1] This effect has been utilized in laser surgery, where femtosecond laser pulses impart negligible damage to surrounding tissues damage as compared with nanosecond laser pulses.[2–7] This property extends beyond biological tissues to a wide variety of materials, including polymers, metals, semiconductors, and insulators.[1] It was previously shown that ablation with ~75 fs, 800 nm laser pulses can remove material from bacterial biofilms and bovine eye tissue with only a minor chemical disruption to the underlayer, in principle allowing depth profiling by subsequent mass spectrometric (MS) analysis in separate instruments.[8,9]

Matrix assisted laser desorption ionization (MALDI) MS imaging of species within organic, polymeric, or biological samples preserves information about their spatial distribution while correlating the ion signal to macroscopic structures.[10,11] Although MALDI-MS is most commonly performed with ns laser pulses, the use of ultrafast (i.e., <2 ps) pulses for intact desorption of biological material promises to greatly extend the sensitivity and spatial resolution of MS imaging. Moreover, the increasing availability of reliable and easily operated ultrafast lasers[1,2] is opening up new possibilities for laser desorption ionization that have not been fully exploited by the MS imaging community. For example, several researchers have begun to use ultrafast laser ablation of biological material for MS applications by either directly forming gaseous ions[12–14] or by desorbing neutral species that are subsequently ionized by electrospray.[15,16] Those studies took advantage of the ability of sub-100 fs laser pulses to induce nonresonant desorption events. Although some of those studies using ultrafast laser pulses for sampling were performed under vacuum, most were done at atmospheric pressure. In parallel, the past decade has experienced a rapid increase in the use of atmospheric pressure desorption ionization methods, including applications for MS imaging.[17–21] These atmospheric pressure-based methods allow the direct analysis of samples while avoiding the dehydrating effects (and resultant structural modifications) of a vacuum. Furthermore, atmospheric pressure sources are readily coupled to the many MS instruments now on the market that display the high mass resolution, accuracy, sensitivity, and tandem capabilities necessary for modern biological analyses.

The present work describes an ultrafast laser ablation time-of-flight mass spectrometer (AToF-MS) that permits imaging at micron-scale resolution and sub-micron-scale depth profiling. The ion source of this instrument can be operated at pressures ranging from 10^{-8} to ~0.3 mbar. Furthermore, mass spectra are collected and stored by the data acquisition system at a 1 kHz rate, which is compatible with standard commercial Ti:sapphire lasers. The capabilities of the AToF-MS instrument are demonstrated using metal foils and semiconductor wafers.

II. EXPERIMENTAL DETAILS

A. Overview of instrument

The experimental setup consists of the following components: a femtosecond laser and associated optics for delivering the laser beam, a high-precision translation stage mounted in a differentially-pumped vacuum chamber, customized ion optics, an ion detector, a high-voltage pulse generator and associated power supplies, and a high-voltage radio frequency (RF) generator. Those components located in or adjacent to the ion source are depicted in Figure 1. Customized controlling software was written using a commercial data acquisition and analysis package.

a)Author to whom correspondence should be addressed. Electronic mail: lhanley@uic.edu.

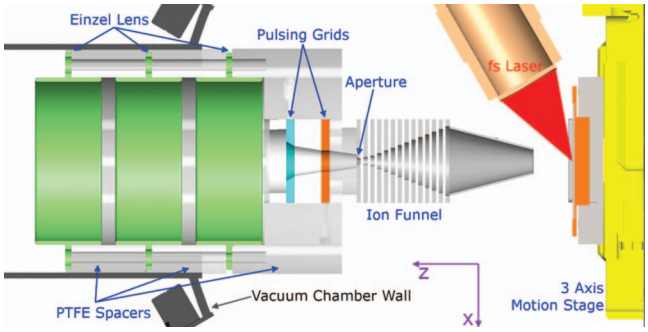

FIG. 1. Illustration of the ion optics, sample stage, laser focus, and vacuum chamber including the differential vacuum wall.

B. Femtosecond laser

Ultrashort laser pulses (800 nm, 45 fs) were generated at a 1 kHz pulse repetition rate by a Ti:sapphire oscillator (Spectra-Physics Tsunami, Newport, Irvine, CA) driven by a diode pumped solid state laser (532 nm, 4.3 Watts, Spectra-Physics Millenia, Newport). The pulses were amplified by a Ti:sapphire regenerative amplifier (Spitfire 50FS, Spectra-Physics) pumped by an Nd:YLF laser (527 nm, Evolution-30, Coherent, Santa Clara, CA). The output of this laser had a near transform-limited bandwidth of 40 nm and a pulse energy of up to 2 mJ. The pulse energy was attenuated to typically 0.1–10 μJ for use in the present experiments by a Rochon polarizer followed by a half-wave plate. The laser pulse passed through a beamsplitter and delay line for future two-pulse experiments. The beam was steered by several mirrors and then focused onto the sample by an infinity-corrected long working distance objective lens (10×/NA0.28, NT59-877, Edmund Optics, Barrington, NJ) mounted inside the ion-source vacuum chamber. The laser pulse energy was measured by a pyroelectric detector (Molectron EPM2000, Coherent, Santa Clara, CA), located near the optical window of the ion source chamber.

The spatial profile was characterized by scanning a knife-edge across the beam, while measuring the transmitted light with a photodiode (FS1010, Thorlabs, Newton, NJ). The knife edge was mounted on a sample plate in front of the photodiode. Multiple z-positions were scanned to find the focal point position. The $1/e^2$ radius of the laser beam was 8 μm at the focal point, and the Rayleigh range was 75 μm. The beam was incident at an angle of 60° from the normal, producing an elliptical, 32×16 μm^2 spot on the target surface. The laser pulse length, measured with an autocorrelator, was 65 fs before entering the optical window of the ion source chamber. The objective lens was estimated to stretch the pulse length to ~75 fs (as measured by inserting a 5-mm thick quartz flat into the beam to simulate the dispersion of the objective).

C. Sample motion stage

Samples were placed on a high-vacuum-compatible 3D motion stage (consisting of three separate PLS-85 stages, Micos USA, Irvine, CA), which allowed movement over a 34×34 mm^2 area with a typical positional resolution of ±0.05 μm. The sample plate holder (45 mm × 45 mm, AB SCIEX, Framingham, MA) was mounted on the motion stage by an insulating polytetrafluoroethylene (PTFE) bracket. A peripheral component interconnect (PCI) bus motor control board (Corvus-PCI, Micos USA, Irvine, CA) was used to drive all three motors directly, with all power and cabling coming from the host computer.

D. Ion optics and detection

The electrically insulated sample plate holder was connected to a custom high voltage pulser (described below) and biased by one channel of a four channel, low ripple power supply (HV-RACK-4-250-00213, UltraVolt, Ronkonkoma, NY). An aluminum cone electrode was used to extract ions from the source region. An ion funnel constructed from 12 aluminum plates insulated by PTFE spacers followed the cone. The plates of the ion funnel were connected via 11 vacuum-compatible resistors (ITT Power Solutions, West Springfield, MA). The first 8 resistors were 2 MΩ, while the three closest to the ToF tube were 3 MΩ. RF was coupled to the ion funnel plates by 10 nF capacitors. The DC gradient on the ion funnel was provided by a floating regulated power supply (Bertan 214, Spellman**,** Hauppauge, NY). RF was generated by a custom-built, high voltage RF generator.[22,23] A gas-limiting aperture plate followed the ion funnel for differential pumping, with a diameter of 1.5 mm. Two high-transmission grids that follow the gas-limiting aperture were used for trapping, selecting, and/or extracting ions when the source chamber was at elevated pressure. The two grids were glued to copper ring plates by vacuum-compatible silver paint and insulated from each other by a machined ceramic piece. The grids and insulating ceramic piece were held by a custom-made PTFE adapter, separating them from the elevated pressure region to prevent high voltage discharge.

Vacuum-compatible Kapton-coated wire passed into the PTFE adapter, connecting the grids to the high voltage pulser. Extra electric insulation on the high voltage feedthroughs in the source region was achieved by vacuum-compatible heat shrinking tubing. This extra insulation was required to prevent high voltage discharge during keV pulsing at ~0.3 mbar pressure, near the Paschen minimum.[24] The custom high voltage pulser used to drive the grids was built from two solid-state high voltage switches (HTS 151-03-GSM, Behlke USA, Billerica, MA), having measured rising and falling times of ~10 ns. Under the high vacuum conditions used in the present study, the grids were grounded, and the ion kinetic energy was defined by the 5–6 keV DC-biased sample plate rather than by the two pulsed grids.

An Einzel lens following the two grids was used to focus ions onto a second, 2.5 mm diam aperture, which provided another stage of differential pumping. A split-lens deflection assembly was used to steer the converging beam through this aperture and towards the detector. DC voltages for the deflectors, ion funnel, cone, and gas-limiting aperture were provided by a six-channel, bipolar power supply (LE-300 vacuum lens controller, Analytica of Branford, Branford, CT). PTFE was used as an insulation and supporting material in between the aluminum Einzel lenses and also as a gas-tight

seal around the outside of the lens stack. The outer diameter of the PTFE spacer was the same as the inner diameter of the vacuum chamber flange, thereby serving as a differential pressure barrier between the source and the ToF region. Polyetheretherketone (PEEK) threaded rods were used to fix the PTFE spacers and Einzel lenses in place under tension, while stainless steel 304 rods were used to connect the high voltage.

Ions that passed through the linear flight tube were detected by a microchannel plate (MCP) detector in an anti-chevron configuration (C-0701, Jordan TOF Products, Grass Valley, CA), normally operated in analog mode because of the high dynamic range of the ablation signals.

E. Differential pumping

For intermediate pressure (10^{-3}–0.3 mbar) experiments, differential pumping was achieved using the two apertures described above: one immediately after the ion funnel and the other close to the detector (not shown). Three ion gauges were installed for vacuum measurement, placed near the detector, inside the flight tube region, and inside the ion source chamber. Two manometers (1.3 mbar maximum, MKS 622B, MKS Instruments, Andover, MA, and 1300 mbar maximum, Datametrics 6000A, Edwards US, Sanborn, NY) were also installed in the source chamber for measuring absolute pressures in the intermediate regime. In the current configuration, six orders of magnitude vacuum isolation were achieved between the source and the detector.

An oil-free scroll pump (Leybold SC15D, Oerlikon Leybold Vacuum USA, Export, PA) was used to evacuate both the flight tube and detector turbomolecular pumps, so that the base vacuum in this foreline routinely remained <0.01 mbar. The dry pump allowed the vacuum to recover to $<10^{-8}$ mbar in just a few hours after venting or inadvertent shutdown, significantly decreasing instrument down time. A standard oil-sealed rotary vane pump was used to back a 300 L/s turbo pump for the ion source chamber.

F. Data acquisition hardware and software

Timing was controlled by a digital pulse delay unit (BNC-565, Berkeley Nucleonics Corporation, San Rafael, CA). This unit was triggered by a 5 VDC pulse from the laser pockels cell driver. The delay unit then triggered the high voltage pulser and the computer data acquisition card. The ion signal was recorded by a PCI digitizer card (8 bit, 1 GS/s, Cobra CS11G8, Gage Applied, Lockport, IL).

Instrument control software was developed entirely in a standard commercial data acquisition and analysis programming environment (LabVIEW, National Instruments, Austin, TX). Customized code was written to ensure the highest possible data transfer rate to the main memory of the computer. Although the data transfer rate was ultimately limited by the PCI bus (effectively 100 MB/s), the digitizer's onboard hardware averaging could be used in many situations to compress significantly the data to be transferred. Data were saved as either text files, when speed was not a concern, or in a custom binary format for high speed streaming.

Separate routines were written to process the raw data, including processing depth profile data and converting customized binary format to BioMAP format (based on Analyze v7.5, www.maldi-msi.org), which was used as the primary MS imaging data analysis software. A special program was written for laser beam profile measurements using the knife-edge approach as described above.

G. Optical microscopy

Two digital single lens reflex cameras (T1i and T2i, Canon USA) were employed for the optical imaging of the sample. The first camera was equipped with a macro lens (normal EF, 50 mm f/2.5 Compact Macro Autofocus Lens, Canon USA) and was used for imaging the entire sample plate. The second camera was mounted behind the objective lens viewport, using a dichroic mirror to deliver the 800 nm laser beam into the objective lens while passing visible light to the camera. This camera was equipped with a 250 mm focal length achromatic doublet lens that formed an image on the camera CCD with a magnification of 12.5×. A kinematic tube mount was used to tilt the camera and lens assembly, so that the laser focus was maintained in the field-of-view. The optical resolution of this arrangement was ∼5 μm, as determined by the use of a resolution target (see the supplementary material).[35]

H. Sample preparation

All metal samples were used as received without any processing. Semiconductor wafers were also used as received except for methanol washing. A resolution test target (Negative 1951 USAF Wheel Pattern Test Target, R3L1S4N, Thorlabs) was also used without further preparation. A tantalum oxide film was prepared on tantalum foil anodically using a standard method.[25] All materials and the resolution test target were adhered to the sample plate inside the mass spectrometer with conductive copper tape.

III. RESULTS AND DISCUSSION

A. Ablation under high vacuum, spatial resolution, and depth profiling

Figure 2(a) shows the laser ablation mass spectra of five elemental metal samples (from bottom to top – Ta, Mo, Cu, Ag, and Au). The surface of each sample was cleaned repetitively by raster scanning under the focused laser beam, after which mass spectra were recorded with 5–6 keV DC bias on the sample plate. All expected metal ions appear in the spectra, with a mass resolution of ∼200. The isotopic distributions were also well represented by the relative intensities of the atomic ions. The Mo^+ peak intensities correlated well with the natural isotope abundances of ^{92}Mo (14.84%), ^{94}Mo (9.25%), ^{95}Mo (15.92%), ^{96}Mo (16.68%), ^{97}Mo (9.55%), ^{98}Mo (24.13%), and ^{100}Mo (9.63%). Reasonable agreement was also observed for the Cu and Ag isotopes.

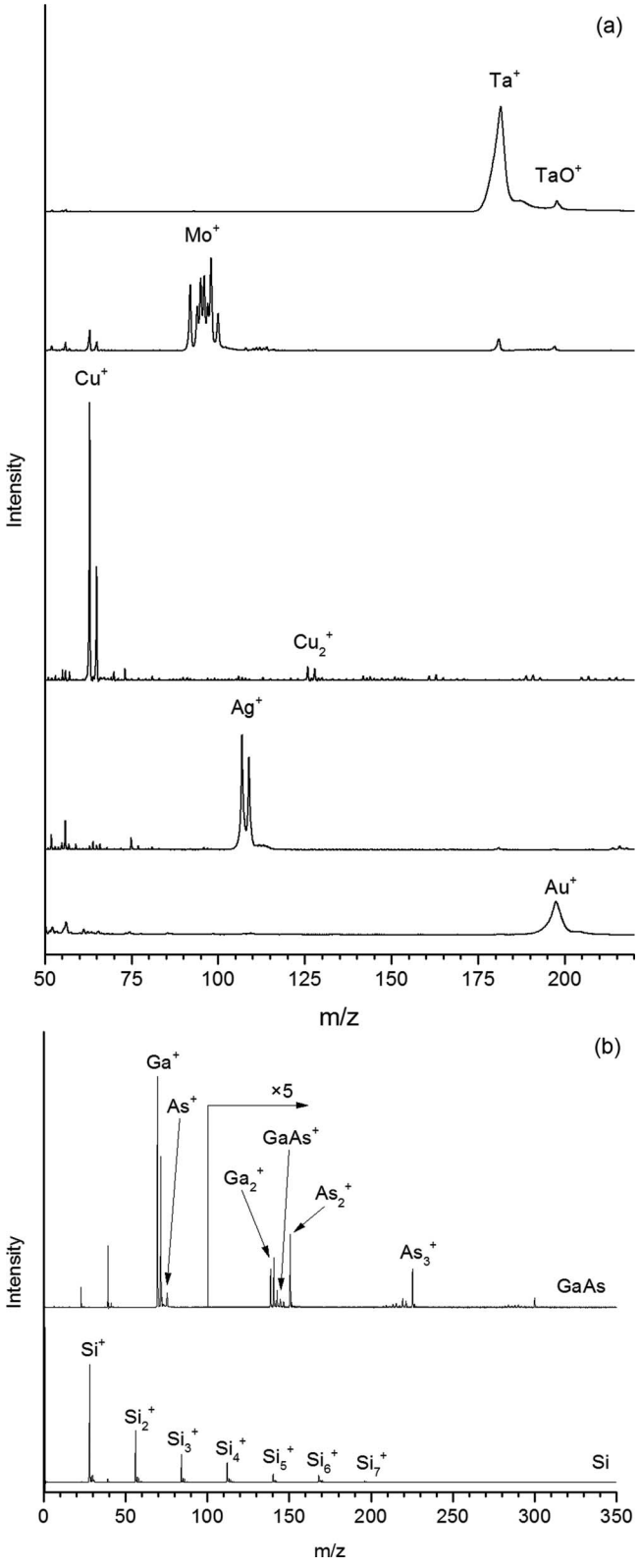

FIG. 2. (a) Laser ablation mass spectra of (from top) Ta, Mo, Cu, Ag, and Au foils at 10^{-6} mbar ambient pressure. (b) Laser ablation mass spectra of (from top) GaAs and Si wafers at 10^{-6} mbar ambient pressure.

Oxygen ions, observed in almost all spectra, resulted from the surface oxide layer that continually reforms at the background pressure of 10^{-6} mbar. Residual carbon was also observed on some samples, as were Cu^{2+} and Ta^{2+} obtained from their respective oxidized metal foils (not shown). Na^+ and K^+ were observed from most samples, as is common in direct laser desorption, because of the low ionization energies of Na and K atoms. Some cross-contamination was observed from deposition of metal that was laser ablated from adjacent samples.

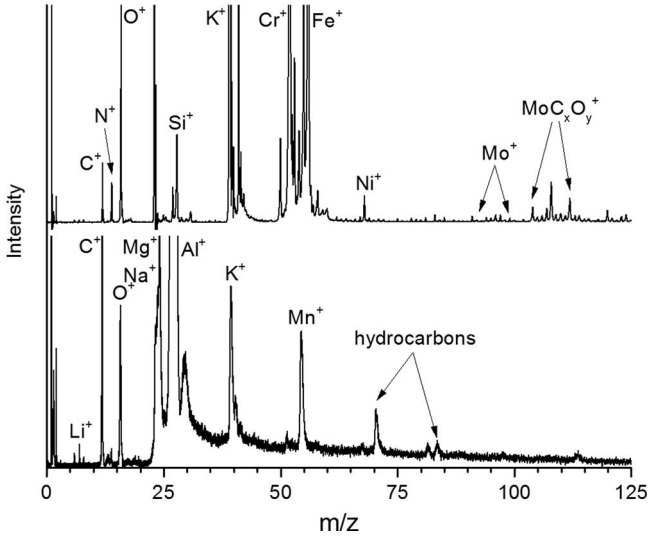

FIG. 3. Laser ablation mass spectra of (top) stainless steel 316 and (bottom) Al 5182 alloy standard.

Figure 2(b) shows laser ablation mass spectra of undoped Si and GaAs wafers, recorded with the laser focused at a fixed position on each sample, recorded at a 1 kHz data acquisition rate. The sample was fixed during data acquisition because the mass resolution was found to be higher without sample scanning. Si^+ and $GaAs^+$ together with their clusters up to $Si_7{}^+$ and $Ga_mAs_n{}^+$ (m+n = 4) were observed. Larger clusters were observed at lower intensity.

Figure 3 shows that Cr^+, Fe^+, Ni^+, and Mo^+ were observed in the laser ablation mass spectrum of stainless steel 316, as expected, because all four elements are major components of this alloy. An Al metal standard (Al5182AS, Alcan) was also analyzed, as shown in Figure 3, to demonstrate the potential for elemental quantification with this instrument. Al^+ and Mg^+ were observed in the spectrum of the Al alloy standard as well as other major alloy components, including Li^+. Mn^+ appeared with a signal-to-noise ratio >10, although it comprises only ~0.3% of the alloy content. These results indicate that the quantification of elemental content from the laser-ablated ion intensity is feasible. Hydrocarbon fragment ions were also observed in the Al alloy mass spectrum.

The USAF test target used to demonstrate the spatial resolution of the instrument was a Cr-coated glass substrate plated with negative resolution patterns. Figure 4(a) is a MS image of Cr^+ signal from the test target, taken with 1 μJ laser pulses with a 32×16 μm^2 elliptical spot size on the surface. Scanning was done in a line-by-line pattern by successively scanning the x-axis of the motion stage and then incrementing the y-axis position. The total acquisition time for this image was 80 min. The image was constructed by setting a nominal pixel size at 5×5 μm^2. All the spectra recorded while the centroid of the laser beam was within a given pixel were averaged together.

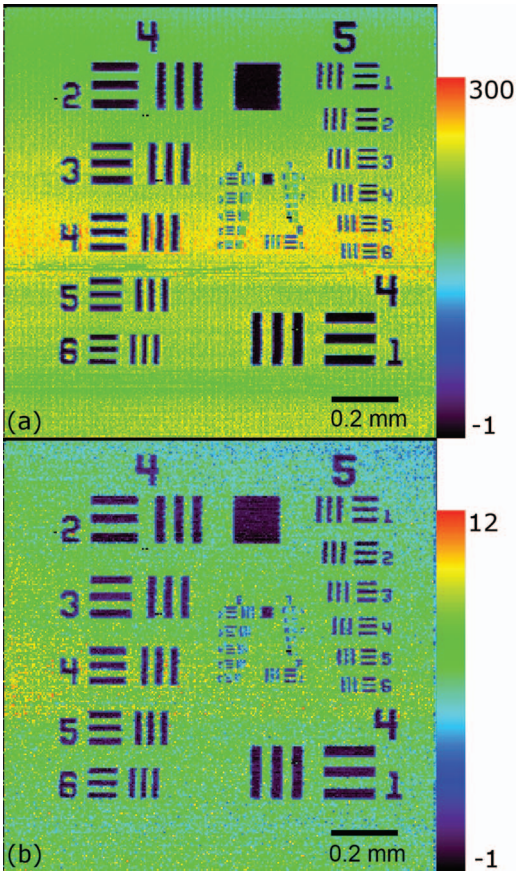

FIG. 4. (a) Cr^+ and (b) $Cr_2{}^+$ mass spectrometric ion images of a USAF test target. Ion intensity bars shown at right with linear integer scales corresponding to ion detector voltage ($-1 = 0$ mV, $300 = 46$ mV, and $12 = 1.8$ mV).

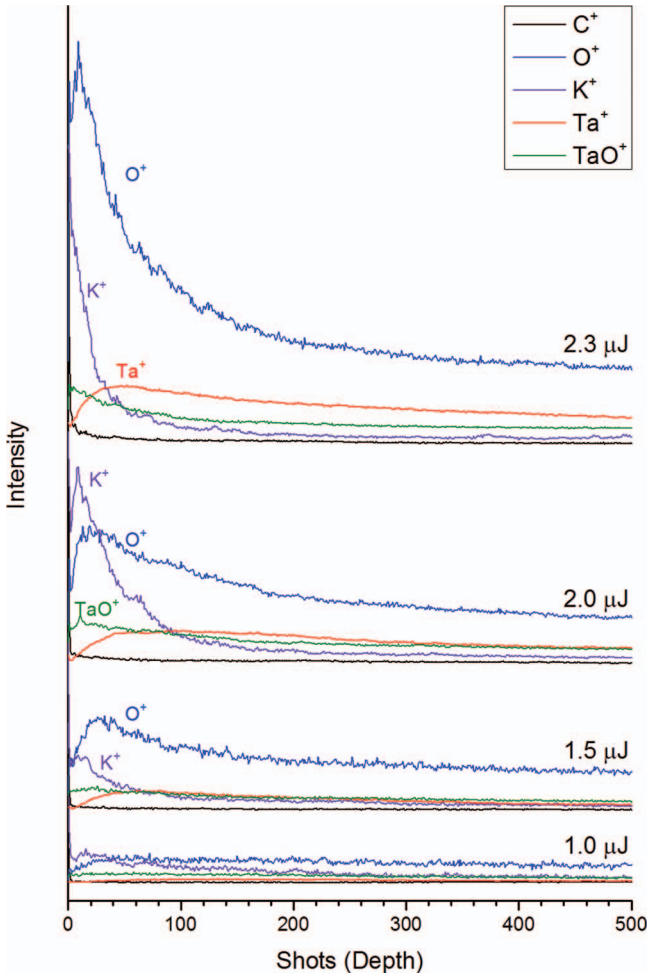

FIG. 5. Ion signal vs. laser shot number at various pulse energies. The data were obtained by ablating a ~330 nm Ta_2O_5 film deposited on Ta foil.

Besides the main Cr^+ peak, the $Cr_2{}^+$ cluster peak was also integrated to construct the image shown in Figure 4(b). The intensity of $Cr_2{}^+$ was only ~5% of the Cr^+ peak, yet both the Cr^+ and $Cr_2{}^+$ images have similar appearance: the group 6 pattern elements are clearly resolved in both images, corresponding to 10 μm spatial resolution. Some vertical strips in group 7 are also resolved, corresponding to ~5 μm spatial resolution. The horizontal resolution was lower than the vertical because of the 60° incident irradiation angle. No effect of the redeposition of Cr on adjacent glass was observed.

The spatial resolution observed was somewhat smaller than the laser spot size, which can be explained by the property that only the center part of the laser beam (TEM_{00}) exceeded the ablation threshold. This effect is a direct consequence of the highly nonlinear ablation process induced by ultrafast near-IR laser pulses, which has been observed in numerous prior studies.[1,2,9] This ability to form craters smaller than the beam diameter has the potential for a dramatic improvement in analytical spatial resolution.[3,9,26,27] A similar effect has also recently been observed in nanosecond laser desorption.[28]

It is vital to determine the laser focal point, the laser spot size, and the Rayleigh range because ultrafast laser ablation is very sensitive to laser fluence. The laser spot size was measured as described in Sec. II B. The beam was fitted to a Gaussian function with the beam radius treated as an adjustable parameter.[9] The laser beam profile was measured at different z-axis positions (moving through the focus), so that the laser spot radius vs. z-axis position was acquired. These results showed that proper sample positioning was crucial while working with the 10× microscope objective lens because of the tight focal range and the correspondingly short Rayleigh range of ~75 μm. Ideally, the thickness of a sample should be measured prior to analysis to a precision of ~20 μm, so that the measured focus can be located as close as possible to the sample surface.

Figure 5 shows the depth profile of a ~330 nm thick Ta_2O_5 film deposited on Ta foil, measured by continuously ablating a fixed area on the sample at a laser repetition rate of 1 kHz. The laser ran for ~1 s to drill each hole, and each spectrum from the digitizer was stored separately, with no averaging, so that ~1000 spectra were recorded for each hole (Figure 5 displays data from the first 500 laser shots only). To improve the statistics, the measurement was repeated on 100 separate spots on the foil and then the data from different spots were averaged according to the laser shot number. Finally, the peak areas corresponding to each element were plotted vs. the number of laser shots, corresponding approximately to the hole depth.

No attempt was made to calibrate the number of laser shots with the actual depth profile of the Ta_2O_5 film. Nevertheless, an estimate of the potential depth resolution can be made by assuming a drop in K^+ signal (which appeared mostly from the surface) to 10% of its initial value. This assumption leads to complete Ta_2O_5 film removal after ~60 laser shots for 2.3 μJ laser energy, the highest used in this study. This result indicates that at this fluence (0.6 J/cm^2), ~6 nm of Ta_2O_5 film was removed per laser shot. The data clearly demonstrate that less material was removed per laser shot at lower laser fluences. By comparison, 30 nm was removed from metallic titanium per laser shot at 1 J/cm^2 fluences using 80 fs, 800 nm laser pulses.[29]

B. Ion funnel and elevated pressure

Variable-pressure experiments were performed by introducing He into the source chamber through a leak valve. The six orders of magnitude of differential pumping between the sample and detection regions of the chamber allowed ~0.3 mbar of He gas to be introduced into the ion source chamber without the collision rate in the ToF drift region or the detector reaching problematic levels.

A Ta sample was used to test the performance of the ion funnel at elevated pressures. Presently, ions can pass through the ion funnel and be extracted into the ToF. Continuing efforts are underway to determine the optimum extraction delay time and extraction voltage for effective ion funneling and ToF operation at elevated pressures.

C. Data acquisition performance

Optimizing the data acquisition throughput of the instrument required significant software development. Many commercial mass spectrometers rely on filtering of pulse-counted data, averaging of many sequential shots, and/or other forms of "on-the-fly" data compression to reduce the data set size prior to storage. The software used here was designed for very rapid data acquisition and did not require use of these strategies. Furthermore, the binary format used for high speed streaming allowed the recording of raw data with minimal data conversion.

For repetitive, short waveforms, such as the 1 kB dataset required for the knife-edge experiment, the data from every shot at the 1 kHz repetition rate laser could be saved to disk without any averaging at the guaranteed 100% capture rate. For medium-length datasets, (i.e., mass spectra up to m/z 650), software averaging was sufficient for acquiring more than 99% of the data or <1% data loss with a longer mass range, but reduced sampling rate on the digitizer (i.e., 250 MS/s). For a longer data set (i.e., 64 kB spectra up to m/z 2500), hardware averaging had to be used to capture >95% of the data at 1 kHz. Future work on the software will address the <0.5% data loss via use of on-board memory.

Overall, the continuous data saving rate was limited by the mechanical hard drive to tens of MB/s. Data were saved in sequence, minimizing disk head movement and maximizing data throughput. For some cases, an idle time was inserted into adjacent instrument operations, so that data buffered in the memory could be saved to disk without averaging at 1 kHz laser repetition rate.

Recent installation of a solid state drive now allows data collection of individual mass spectra collected at the full 1 kHz repetition rate without the need for hardware averaging prior to transfer. The software is also capable of providing more functions when hardware averaging is bypassed. Spectra acquired directly by the digitizer can be processed on-the-fly by multiple digital filters such as *software*-based pulse counting, time-to-digital conversion, and electronic noise removal. Such digital filters can help reveal weak signals in a noisy background.

When these techniques are not required, hardware averaging provides the benefit of substantial decrease in data transfer over the system bus, and data acquired at laser pulse repetition rates of 1 kHz could be transferred to computer memory and saved continuously with negligible loss.

While it is taxing on the data transfer process, the 1 kHz repetition rate of the laser allowed rapid imaging. For example, a 100×100 pixel image with 50 mass spectra averaged per pixel required only 15 min to acquire and an additional 2 min to convert to BioMAP format for analysis. Because of the efficient binary data format, an image with 256×256 pixels per spectrum and a data length of 32 kB could be processed in 2 min, generating a 600 MB BioMAP MS image. Another measure of the rapid data processing was that a depth profile of a 10×10 array of laser-drilled holes required only ~2 min for collection with another 2 min for data processing. Knife-edge measurements of the beam profile could be completed within 20 min, facilitating optical characterization.

IV. CONCLUSIONS

The AToF-MS described here can rapidly collect two-dimensional ion images of elemental species with micron-scale resolution. Additionally, the use of ultrafast laser ablation holds the promise of submicron spatial resolution for depth profiling and three dimensional imaging. The highly efficient data acquisition permits data storage with little loss and without the need for averaging even at 1 kHz, matching the repetition rate of Ti:sapphire lasers.

The ion funnel allows the source to operate at pressures up to ~0.3 mbar. Work is underway to optimize collection of laser ablation MS at elevated pressures, to combine the advantages of atmospheric MS[17–21] with those of femtosecond laser desorption[12–16] A common linear, reflectron, and orthogonal ToF design could have been used here to provide higher sensitivity at high vacuum,[30] but would not allow the collection of MS at elevated pressures that will be possible with the AToF-MS design. The AToF-MS should also allow collisional cooling of the high kinetic energy ions formed by femtosecond laser ablation,[30] improving mass resolution.

Femtosecond laser ablation ToF-MS has been described as a semiquantitative method for spatially resolved elemental analysis because ion yields do vary with element and sample characteristics.[30] For this reason, most prior work on elemental analysis by femtosecond laser ablation has been coupled with inductively coupled plasma (ICP) MS.[30–32] The

former samples the ions formed directly by laser ablation while the latter samples mostly nanoparticles, with atomic ions probably not detected. A thorough comparison of the two methods is beyond the scope of this work, but a quick comparison shows both methods can readily detect major and minor elements in metallic alloys.[33] Quantification is better established in ICP-MS, but is typically achieved from much more defocused laser beams than employed here. Overall, the use of appropriate standards should permit at least approximate quantification with the AToF-MS in metallic alloys and semiconductors. The AToF-MS has the potential advantages for the elemental analysis of higher spatial resolution and simpler instrumental configuration than ICP-MS.

Finally, installation of a 10.5 eV vacuum ultraviolet source on the AToF-MS for single-photon ionization is ongoing and will allow collection of MS of ultrafast laser ablated neutrals for molecular imaging of a wide variety of synthetic and biological samples.[9,15,16,34]

ACKNOWLEDGMENTS

Custom hardware was machined by Francisco M. Tobias, Francisco Alvarez, and Joseph Dublin of the UIC Chemistry machine shop. Custom electronics were built by Don Rippon of the UIC Chemistry electronics shop. This work was supported by the National Institute of Biomedical Imaging and Bioengineering (Grant No. EB006532), the U.S. Air Force Surgeon General's Office of Modernization (Contract No. FA7014-07-C-0047), and the University of Illinois at Chicago. The contents of this manuscript are solely the responsibility of the authors and do not necessarily represent the official views of the National Institute of Biomedical Imaging and Bioengineering, the National Institutes of Health, or the U.S. Air Force Surgeon General's Office of Modernization.

[1] R. F. Gattass and E. Mazur, Nat. Photonics **2**, 219 (2008).
[2] A. Vogel, J. Noack, G. Huttman, and G. Paltauf, Appl. Phys. B **81**, 1015 (2005).
[3] S. Maxwell and E. Mazur, Med. Laser Appl. **20**, 193 (2005).
[4] S. Toyran, Y. Liu, S. Singha, S. Shan, M. R. Cho, R. J. Gordon, and D. P. Edwards, Exp. Eye Res. **81**, 298 (2005).
[5] Y. Liu, S. Sun, S. Singha, M. R. Cho, and R. J. Gordon, Biomaterials **26**, 4597 (2005).
[6] Y. Liu, H. Nakamura, T. E. Witt, D. P. Edward, and R. J. Gordon, Ophthalmic Surg. Lasers Imaging **39**, 485 (2008).
[7] H. Nakamura, Y. Liu, T. E. Witt, D. P. Edward, and R. J. Gordon, Invest. Ophthalmol. Vis Sci. **50**, 1198 (2009).
[8] S. Milasinovic, Y. Liu, G. L. Gasper, Y. Zhao, J. L. Johnston, R. J. Gordon, and L. Hanley, J. Vac. Sci. Technol. A **28**, 647 (2010).
[9] S. Milasinovic, Y. Liu, C. Bhardwaj, M. Blaze M. T., R. J. Gordon, and L. Hanley, Anal. Chem. **84**, 3945 (2012).
[10] K. Chughtai and R. M. A. Heeren, Chem. Rev. **110**, 3237 (2010).
[11] E. H. Seeley and R. M. Caprioli, Anal. Chem. **84**, 2105 (2012).
[12] J. I. Berry, S. Sun, Y. Dou, A. Wucher, and N. Winograd, Anal. Chem. **75**, 5146 (2003).
[13] J. M. Wichmann, C. Lupulescu, L. Wöste, and A. Lindinger, Rapid Commun. Mass Spectrom. **23**, 1105 (2009).
[14] Y. Coello, A. D. Jones, T. C. Gunaratne, and M. Dantus, Anal. Chem. **82**, 2753 (2010).
[15] J. J. Brady, E. J. Judge, and R. J. Levis, Rapid Commun. Mass Spectrom. **23**, 3151 (2009).
[16] E. J. Judge, J. J. Brady, D. Dalton, and R. J. Levis, Anal. Chem. **82**, 3231 (2010).
[17] V. V. Laiko, S. C. Moyer, and R. J. Cotter, Anal. Chem. **72**, 5239 (2000).
[18] D. J. Weston, Analyst **135**, 661 (2010).
[19] D. R. Ifa, C. Wu, Z. Ouyang, and R. G. Cooks, Analyst **135**, 669 (2010).
[20] P. Nemes, A. S. Woods, and A. Vertes, Anal. Chem. **82**, 982 (2010).
[21] A. S. Galhena, G. A. Harris, L. Nyadong, K. K. Murray, and F. M. Fernandez, Anal. Chem. **82**, 2178 (2010).
[22] R. M. Jones, D. Gerlich, and S. L. Anderson, Rev. Sci. Instrum. **68**, 3357 (1997).
[23] R. M. Jones and S. L. Anderson, Rev. Sci. Instrum. **71**, 4335 (2000).
[24] P. Osmokrovic and A. Vasic, IEEE Trans. Plasma Sci. **33**, 1672 (2005).
[25] R. E. Pawel, Rev. Sci. Instrum. **35**, 1066 (1964).
[26] S. Kuper and M. Stuke, Appl. Phys. Lett. **54**, 4 (1989).
[27] K. Konig, I. Riemann, and W. Fritzsche, Opt. Lett. **26**, 819 (2001).
[28] O. Kostko, L. K. Takahashi, and M. Ahmed, Chem. Asian J. **6**, 3066 (2011).
[29] M. Ye and C. P. Grigoropoulos, J. Appl. Phys. **89**, 5183 (2001).
[30] R. Hergenroder, O. Samek, and V. Hommes, Mass Spectrom. Rev. **25**, 551 (2006).
[31] J. Pisonero and D. Gunther, Mass Spectrom. Rev. **27**, 609 (2008).
[32] J. Koch and D. Gunther, Appl. Spectrosc. **65**, 155A (2011).
[33] H. Wiltsche and D. Gunther, Anal. Bioanal. Chem. **399**, 2167 (2011).
[34] A. Akhmetov, J. F. Moore, G. L. Gasper, P. J. Koin, and L. Hanley, J. Mass Spectrom. **45**, 137 (2010).
[35] See supplementary material at http://dx.doi.org/10.1063/1.4750974 for laser beam profile and optical resolution of AToF-MS.